Supporting information for

Modeling semi-batch vinyl acetate polymerization processes

Andreas Feuerpfeil[1], Marco Drache[1], Laura-Alice Jantke[2], Timo Melchin[2], Jessica Rodríguez-Fernández[2], Sabine Beuermann[1*]

[1] Clausthal University of Technology, Institute of Technical Chemistry, Arnold-Sommerfeld-Straße 4, 38678 Clausthal-Zellerfeld, Germany

[2] Wacker Chemie AG, Johannes-Hess-Str. 24, 84489 Burghausen, Germany

* sabine.beuermann@tu-clausthal.de

Table S1: Physical properties of the substances in the reaction mixture

substance	molar mass / g mol^{-1}	density / kg m^3
vinyl acetate[1]	86.09	ρ = 959.3 – 1.34 * T (in °C)
methanol[2]	32.04	$\rho = \frac{A}{B^{1+\left(1-\frac{T}{C}\right)^D}}$ A = 54.566, B = 0.233211, C = 513.16, D = 0.20887 T in K
tert-butyl peroxypivalate[3]	174.2	-
poly(vinyl acetate)[1]	-	ρ = 1209.4 – 0.49 * T (in °C)

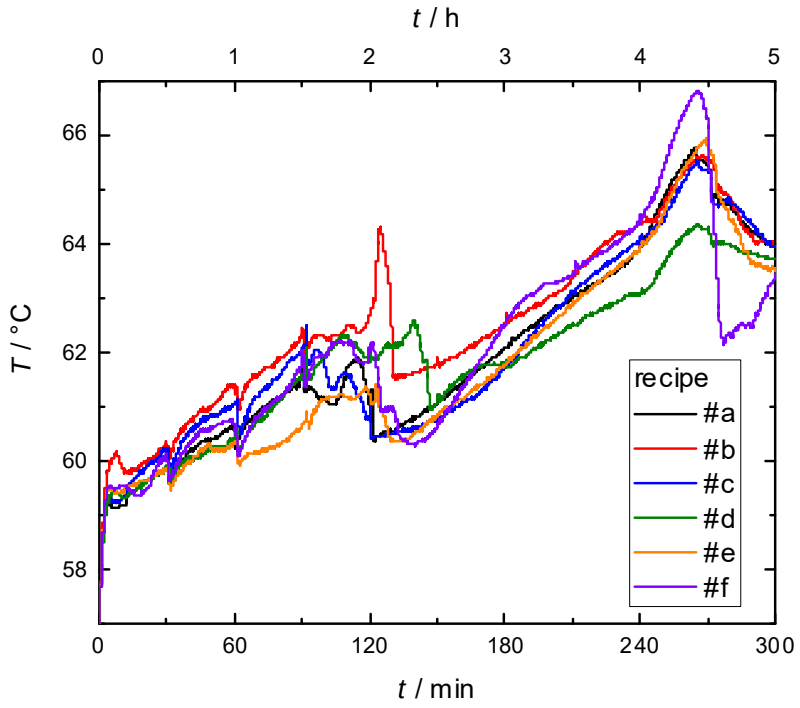

Figure S1: Temperature profiles for the recipes given in Table 1 of the main text. The temperatures are coupled with the actual composition of the reaction mixtures

Determination of transfer coefficients based on literature data

The transfer constants and the propagation rate coefficient of macromonomers with terminal double bonds are taken from the literature. In Figures S2, S3 and S4 the Arrhenius diagrams are shown for the transfer rate coefficients, converted from the transfer constants in the original publications. For the transfer to polymer reactions the difference in the activation energies of the transfer and the propagation reaction was given by Nozakura et al.[4] To determine the pre-exponential factors the given activation energies were converted into slopes in the linear Arrhenius diagram (Figure S2 and S3). In Figure S5 the Arrhenius diagram of the propagation rate coefficient of a macromonomer is illustrated. The Arrhenius diagram shown is calculated with the reactivity factor *K* of the original publication.

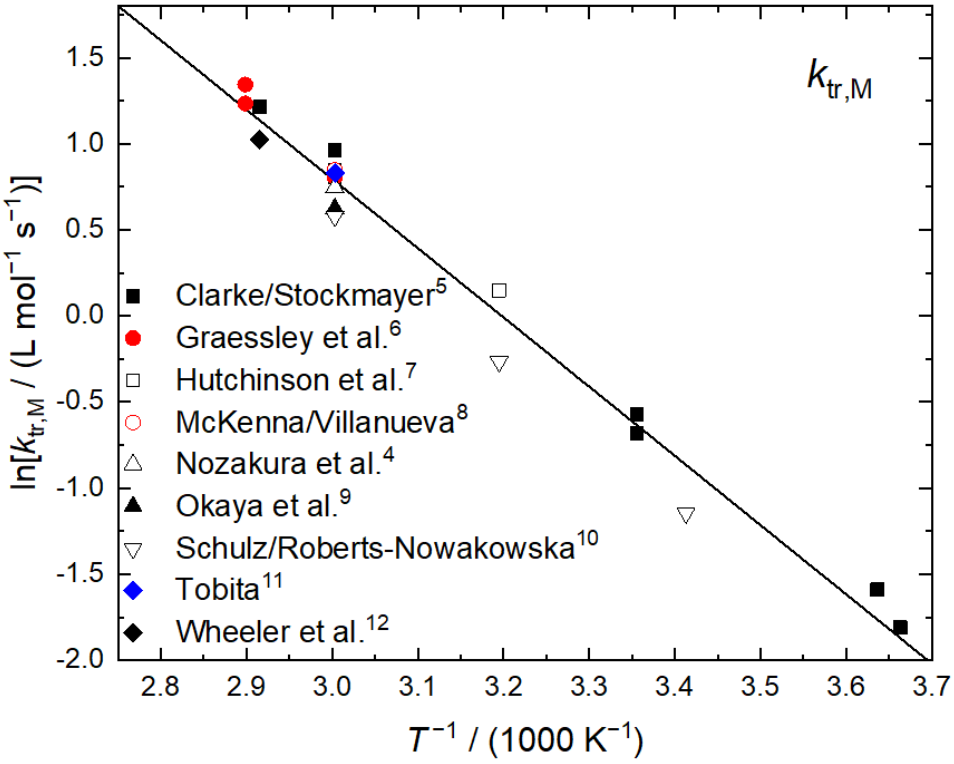

Figure S2: Arrhenius diagram of the transfer to the monomer rate coefficient. Pre-exponential factor $A = 3.85 \cdot 10^5$ L mol^{-1} s^{-1}. Activation energy $E_a = 33.4$ kJ mol^{-1}.[4–12]

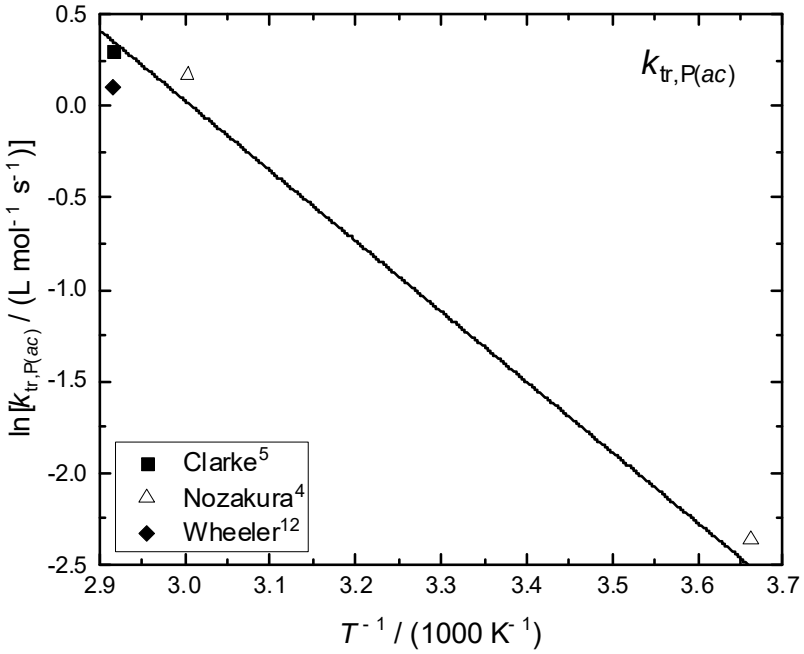

Figure S3: Arrhenius diagram of the transfer to polymer on the acetate group rate coefficient. Pre-exponential factor $A = 1.03 \cdot 10^5$ L mol^{-1} s^{-1}. Activation energy $E_a = 31.9$ kJ mol^{-1}.[4,5,12]

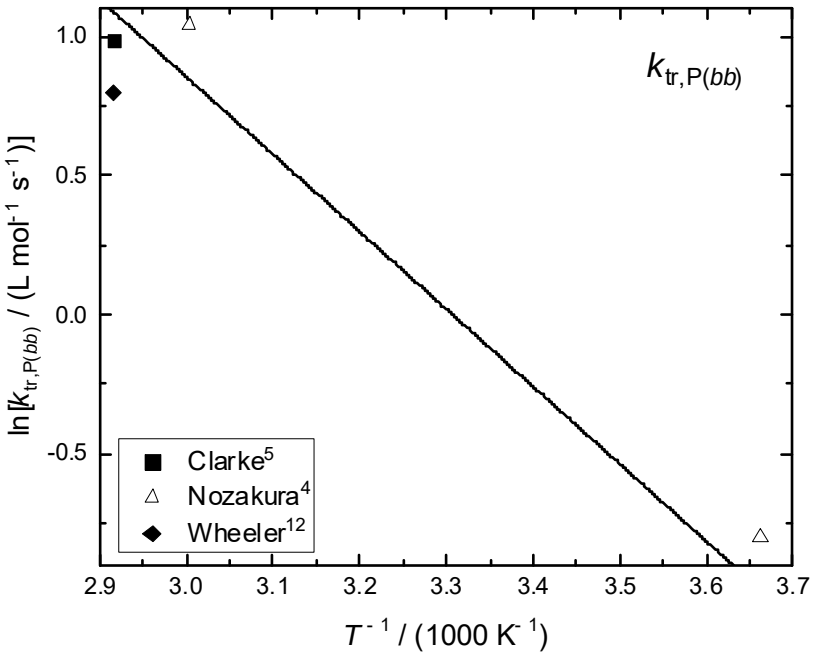

Figure S4: Arrhenius diagram of the transfer to polymer on the backbone rate coefficient. Pre-exponential factor $A = 9.82 \cdot 10^3$ L mol^{-1} s^{-1}. Activation energy $E_a = 23.1$ kJ mol^{-1}.[4,5,12]

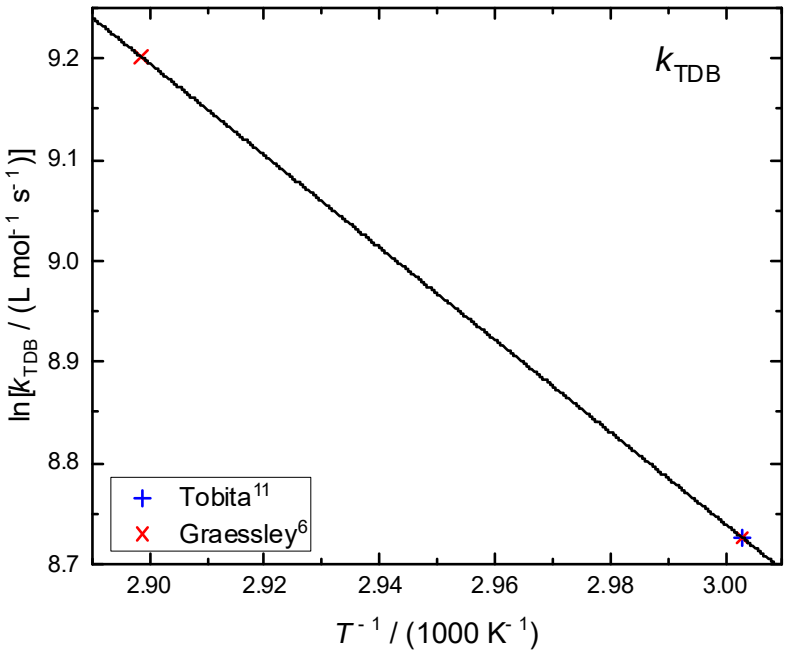

Figure S5: Arrhenius diagram of the macromonomer propagation rate coefficient. Pre-exponential factor $A = 5.39 \cdot 10^9$ L mol^{-1} s^{-1}, activation energy $E_a = 37.9$ kJ mol^{-1}.[6,11]

Comparison of equation (S1, 4 of the main text) and (S3, 6 of the main text) for the case of a low P_2 or a high P_3 value

In the case of a low P_2 or a high P_3 value the $k_t^{1,1}$ value at zero solids content is noticeably lowered. To prevent this behavior, equation (S3) was introduced. The comparison of equation (S1) and (S3) (see below) is shown in Figure S6: the orange and the solid black curve were calculated with the same parameter values, but equation (S1) (orange) starts below the normalized $k_t^{1,1}$-value, while equation (S3) starts as expected at 1.

$$k_t^{1,1} = k_t^{1,1}(X' = 0) \cdot \frac{1 - P_1 \cdot X'}{1 + \exp\left(\frac{X' - P_2}{P_3}\right)} \tag{S1}$$

$$P_0 = 1 + \exp\left(\frac{-P_2}{P_3}\right) \tag{S2}$$

$$k_t^{1,1} = k_t^{1,1}(X' = 0)\frac{P_0 - P_1 \cdot X'}{1 + \exp\left(\frac{X' - P_2}{P_3}\right)} = k_t^{1,1}(X' = 0)\frac{1 + \exp\left(\frac{-P_2}{P_3}\right) - P_1 \cdot X'}{1 + \exp\left(\frac{X' - P_2}{P_3}\right)} \tag{S3}$$

The influence of P_1 is illustrated with the black and the red curves. The black curves have the same values of the parameters, but for the dashed curve P_1 was set to $P_1 = 0$. The red dotted curve matches the black solid curve and demonstrates that the shape of the black solid curve is not determined by P_1.

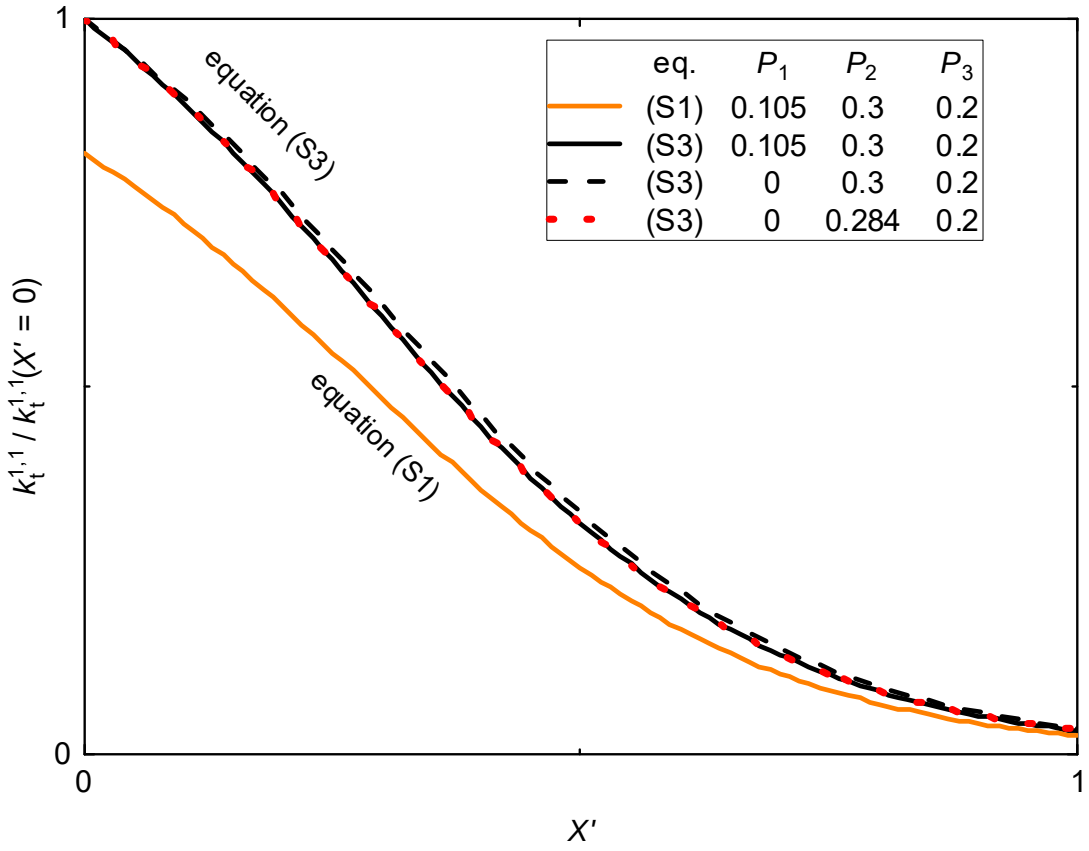

Figure S6: Variation of $k_t^{1,1} / k_t^{1,1}(X' = 0)$ with increasing solids content. Orange curve calculated with equation (S1), black and red curves calculated with equation (S3). The parameters of the curves shown are freely chosen. It is demonstrated that the use of equation (S1) can lead to considerable deviations from the literature value of $k_t^{1,1}$. Furthermore, it is shown that for a low P_2 and a high P_3 value, P_1 hardly influences the shape of the curve.

Automated parameter search

The automated parameter search is executed by a *Metropolis-Hasting* algorithm.[13,14] The Python code used is illustrated in Figure S7 and explained below. The algorithm implemented is based on two classes: fit and model.

1. The initial values (**initValue**) needed for the first loop/cycle are stored in the vector **fit.init**. Additionally, the vector contains the associated lower and upper limits (**minValue**; **maxValue**, respectively) and the parameter **relSigma** (0.05) that controls the parameter variation (mutation).
2. The parameter optimization starts in the model class with the values defined in **initValue** (**currentValues**).
3. **model.setValues()**: transfer of the **currentValues** into the kinetic model of the 6 experiments (#a – #f)
4. **model.run()**: simultaneous start of the simulation of all experiments with their individual recipe
5. **model.wait()**: delay of the next step until all simulations are finished (synchronization)
6. **model.diff2()**: comparison of the 6 simulations with the corresponding experimental solids contents.
7. **fit.accept()**: accept or discard the current parameter set. 4 cases may occur:
   (I) first cycle,
   (II) $diff_1^2 < diff_0^2$,
   (III) $diff_0^2 / diff_1^2 >$ random number r ($0 \leq r \leq 1$) and
   (IV) $diff_0^2 / diff_1^2 <$ random number r ($0 \leq r \leq 1$).
   Cases (I) – (III): **currentValues** are accepted and $diff_0^2$ is set equal to $diff_1^2$.
   Case (IV) **currentValues** are discarded, $diff_0^2$ as reference remains unchanged, last record is reused as **currentValue**.
8. **fit.mutation()**: Generation of a new parameter set by mutation considering the lower and upper bounds; The width is determined using a Gaussian density distribution of the standard deviation **relSigma** * (**maxValue** – **minValue**) → new **currentValues**
9. New optimization cycle starts at step 3 **model.setValues()**

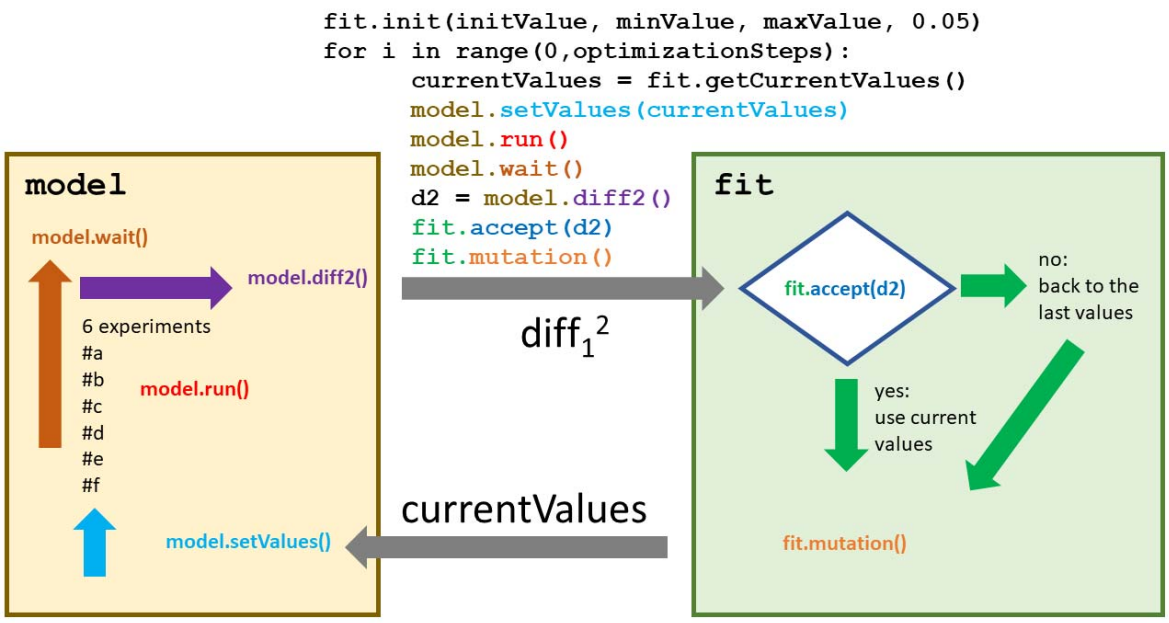

Figure S7: Scheme of the automated parameter search. The search is organized in the model class (left) and the fit class (right). The current values of the k_t model is transferred to the kinetic model and the simulations are executed simultaneously and parallelized in the model class. In the fit class the simulations are compared with the last ones to decide if the values found are accepted or discarded. For further information please refer to the text.

Molar mass distributions

The molar mass distributions of experiments #a - #f are shown in Figure S8. The molar mass distribution of experiment #b is omitted, because of discrepancies in the time allocation.

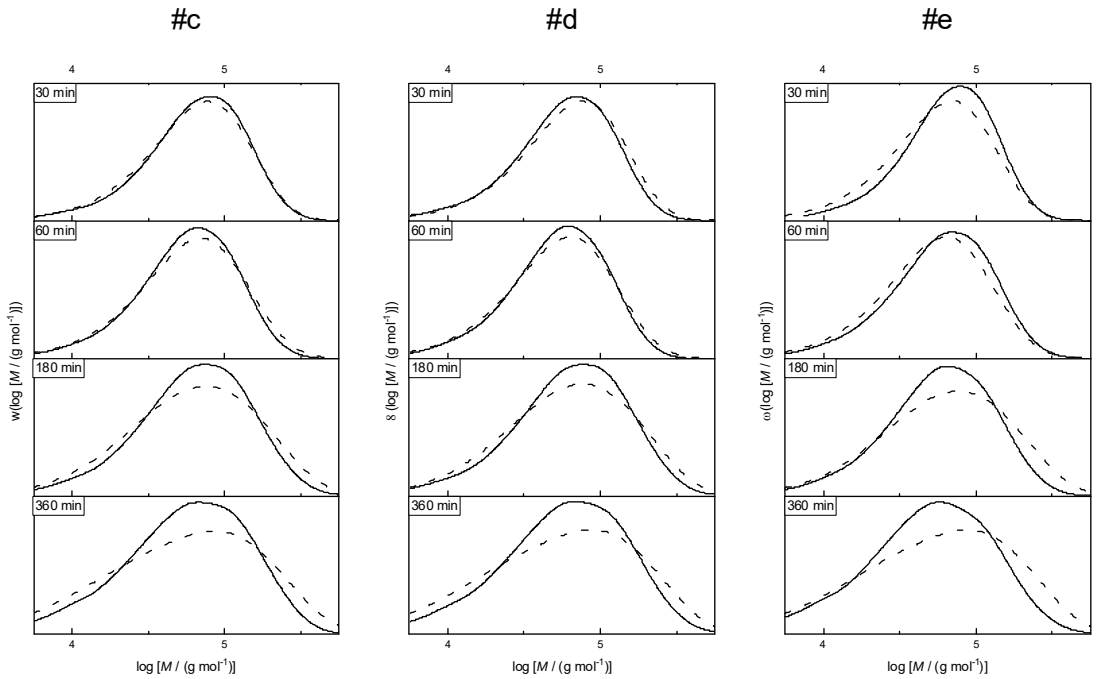

Figure S8: Molar mass distributions of the recipes #c, #d and #e. Solid curves: experimental data; dashed lines: simulated data.

Molar mass averages and dispersities

Table S2: Experimental and simulated molar mass averages and dispersities of recipe #a.

time / min	experiment			simulation		
	M_n / (g mol$^{-1)}$	M_w / (g mol^{-1})	$Đ$	M_n / (g mol^{-1})	M_w / (g mol^{-1})	$Đ$
30	56400	95600	1.69	46900	96900	2.07
60	51900	88000	1.70	41900	91700	2.19
90	49600	91500	1.84	41500	96300	2.32
120	50800	94600	1.86	39900	101000	2.52
150	48300	94800	1.96	36700	103000	2.81
180	47200	93700	1.98	32300	104000	3.21
210	41000	93500	2.28	27800	104000	3.73
240	39100	88300	2.26	24000	103000	4.29
270	36600	87800	2.40	20100	102000	5.08
300	32100	89900	2.80	17200	102000	5.93
330	33100	86900	2.63	15400	102000	6.61
360	33300	86100	2.58	14500	102000	7.01

Table S3: Experimental and simulated molar mass averages and dispersities of recipe #b.

time / min	experiment			simulation		
	M_n / (g mol^{-1})	M_w / (g mol^{-1})	$Đ$	M_n / (g mol^{-1})	M_w / (g mol^{-1})	$Đ$
30	48700	87200	1.79	42600	87900	2.06
60	41600	77200	1.86	38200	83000	2.17
120	38800	84400	2.18	37600	93300	2.48
180	39600	77000	1.95	30500	96100	3.15
240	27400	75700	2.77	23200	95300	4.11
300	30700	71300	2.32	16900	94400	5.58
360	28500	69400	2.43	14000	94200	6.71

Table S4: Experimental and simulated molar mass averages and dispersities of recipe #c.

time / min	experiment			simulation		
	M_n / (g mol^{-1})	M_w / (g mol^{-1})	$Đ$	M_n / (g mol^{-1})	M_w / (g mol^{-1})	$Đ$
30	44500	81800	1.84	39200	80700	2.06
60	39700	72100	1.82	35200	76100	2.16
120	44000	87100	1.98	36500	88800	2.43
180	38500	86000	2.24	31800	94300	2.96
240	36600	84800	2.32	24200	94700	3.92
300	33000	84100	2.55	17300	94000	5.42
360	31900	81300	2.55	14500	93800	6.47

Table S5: Experimental and simulated molar mass averages and dispersities of recipe #d.

time / min	experiment			simulation		
	M_n / (g mol^{-1})	M_w / (g mol^{-1})	$Đ$	M_n / (g mol^{-1})	M_w / (g mol^{-1})	$Đ$
30	49900	80700	1.62	38600	79200	2.05
60	41600	75600	1.82	34900	74700	2.14
120	39800	76800	1.93	34600	82400	2.38
180	39000	76700	1.97	29100	84000	2.89
240	34500	77800	2.25	22800	82900	3.64
300	31600	71700	2.27	16700	81800	4.89
360	26500	71700	2.70	13600	81600	6.02

Table S6: Experimental and simulated molar mass averages and dispersities of recipe #e.

time / min	experiment			simulation		
	M_n / (g mol^{-1})	M_w / (g mol^{-1})	$Đ$	M_n / (g mol^{-1})	M_w / (g mol^{-1})	$Đ$
30	39900	72900	1.83	34800	71500	2.05
60	37600	66100	1.76	31700	67900	2.14
120	41800	83300	1.99	36200	85600	2.37
180	42200	87800	2.08	32500	93300	2.87
240	37200	87200	2.34	24800	94200	3.8
300	30800	86300	2.80	17700	93600	5.3
360	32900	84300	2.56	14700	93400	6.37

Table S7: Experimental and simulated molar mass averages and dispersities of recipe #f.

time / min	experiment			simulation		
	M_n / (g mol^{-1})	M_w / (g mol^{-1})	$Đ$	M_n / (g mol^{-1})	M_w / (g mol^{-1})	$Đ$
30	38100	65900	1.73	31500	64500	2.05
60	32500	59200	1.82	28800	61400	2.13
120	43600	90500	2.08	34200	80700	2.36
180	46200	96300	2.09	31300	88500	2.83
240	35200	85200	2.42	23900	89500	3.75
300	35300	85400	2.42	17300	89000	5.14
360	29300	85800	2.93	14400	88900	6.17

References

(1) Barudio, I.; Févotte, G.; McKenna, T. F. L. Density data for copolymer systems: butyl acrylate/vinyl acetate homo- and copolymerization in ethyl acetate. *European Polymer Journal* **1999**, *35* (5), 775–780. DOI: 10.1016/S0014-3057(98)00070-6.

(2) DDBST GmbH. *Liquid Density Calcualtion by DIPPR105 Equation (Methanol)*. http://ddbonline.ddbst.com/DIPPR105DensityCalculation/DIPPR105CalculationCGI.exe?component=Methanol&tunit=K&punit=kg%2Fm3&TemperaturesEdit=&calculate=Calculate (accessed 2021-06-09).

(3) Akzo Nobel. *Initiators*:*Initiators for High Polymers*. http://www.neochemical.kz/File/Akzo_Data_110407-Initiators_for_High_Polymers.pdf (accessed 2021-03-09).

(4) Nozakura, S.-I.; Morishima, Y.; Murahashi, S. Long branching in poly(vinyl acetate) and poly(vinyl alcohol). III. Kinetic study of the branching reaction in the radical polymerization of vinyl acetate. *J. Polym. Sci. A-1 Polym. Chem.* **1972**, *10* (10), 2853–2866. DOI: 10.1002/pol.1972.170101004.

(5) Clarke, J. T.; Howard, R. O.; Stockmayer, W. H. Chain Transfer in Vinyl Acetate Polymerization. *Macromol. Chem. Phys.* **1961**, *44* (1), 427–447. DOI: 10.1002/macp.1961.020440136.

(6) Graessley, W. W.; Hartung, R. D.; Uy, W. C. Studies of branching in polyvinyl acetate. *J. Polym. Sci. A-2 Polym. Phys.* **1969**, *7* (11), 1919–1935. DOI: 10.1002/pol.1969.160071107.

(7) Hutchinson, R. A.; Richards, J. R.; Aronson, M. T. Determination of Propagation Rate Coefficients by Pulsed-Laser Polymerization for Systems with Rapid Chain Growth: Vinyl Acetate. *Macromolecules* **1994**, *27* (16), 4530–4537. DOI: 10.1021/ma00094a016.

(8) McKenna, T. F. L.; Villanueva, A. Effect of solvent on the rate constants in solution polymerization. Part II. Vinyl acetate. *J. Polym. Sci. A Polym. Chem.* **1999**, *37* (5), 589–601. DOI: 10.1002/(SICI)1099-0518(19990301)37:5<589::AID-POLA8>3.0.CO;2-1.

(9) Okaya, T.; Kikuchi, K.; Suzuki, A.; Ikeda, N. Dispersion polymerization of vinyl acetate in a mixture of ethanol and water. *Polym. Int.* **2005**, *54* (1), 143–148. DOI: 10.1002/pi.1658.

(10) Schulz, V. G. V.; Roberts-Nowakowska, L. Über die Temperaturabhängigkeit einiger Übertragungskonstanten der radikalischen Polymerisation von Vinylacetat:Über die Verzweigung des Polyvinylacetats, IV. *Makromol. Chem.* **1964**, *80* (1), 36–43. DOI: 10.1002/macp.1964.020800104.

(11) Tobita, H. A simulation model for long-chain branching in vinyl acetate polymerization: 2. Continuous polymerization in a stirred tank reactor. *J. Polym. Sci. B Polym. Phys.* **1994**, *32* (5), 911–919. DOI: 10.1002/polb.1994.090320514.

(12) Wheeler, O. L.; Lavin, E.; Crozier, R. N. Branching mechanisms in the polymerization of vinyl acetate. *J. Polym. Sci.* **1952**, *9* (2), 157–169. DOI: 10.1002/pol.1952.120090204.

(13) Metropolis, N.; Rosenbluth, A. W.; Rosenbluth, M. N.; Teller, A. H.; Teller, E. Equation of State Calculations by Fast Computing Machines. *J. Chem. Phys.* **1953**, *21* (6), 1087–1092. DOI: 10.1063/1.1699114.

(14) Hastings, W. K. Monte Carlo sampling methods using Markov chains and their applications. *Biometrika* **1970**, *57* (1), 97–109. DOI: 10.1093/biomet/57.1.97.